

Corrections

NEUROSCIENCE. For the article “Development of ^{17}O NMR approach for fast imaging of cerebral metabolic rate of oxygen in rat brain at high field,” by Xiao-Hong Zhu, Yi Zhang, Run-Xia Tian, Hao Lei, Nanyin Zhang, Xiaoliang Zhang, Hellmut Merkle, Kamil Ugurbil, and Wei Chen, which appeared in number 20, October 1, 2002, of *Proc. Natl. Acad. Sci. USA* (**99**, 13194–13199; First Published September 19, 2002; 10.1073/pnas.202471399), the authors note the following correction. After the publication of this article, the authors found a technical error in the setup of parameters used for acquiring the 3D ^{17}O magnetic resonance spectroscopic (MRS) images reported in this article. This error led to overestimations of the spatial resolution of 3D ^{17}O MRS images. The claimed voxel sizes of the 3D ^{17}O MRS images (Figs. 2 and 3) and the cerebral metabolic rate of oxygen (CMRO₂) image (Fig. 6) are 57% smaller than the actual voxel size in each spatial dimension. Therefore, the correct voxel size was 0.10 ml, and the correct field-of-view (FOV) used in the 3D ^{17}O MRS images was $28 \times 28 \times 24 \text{ mm}^3$. This correction should not significantly affect the major conclusions and methodology presented in this article. However, the correction could reveal that the current sensitivity of ^{17}O NMR and, alternatively, the spatial resolution of the ^{17}O MRS image achieved at 9.4 tesla may be potentially limited for determining and imaging CMRO₂ in small brain structures such as the white matter in the rat brain.

www.pnas.org/cgi/doi/10.1073/pnas.0837868100

COLLOQUIUM. For the colloquium paper “Unified scaling law for earthquakes,” by Kim Christensen, Leon Danon, Tim Scanlon, and Per Bak, which appeared in Suppl. 1, February 19, 2002, of *Proc. Natl. Acad. Sci. USA* (**99**, 2509–2513), and for the *Physical Review Letters* paper “Unified Scaling Law for Earthquakes,” by Per Bak, Kim Christensen, Leon Danon, and Tim Scanlon, which appeared April 29, 2002, in *Phys. Rev. Lett.* (**88**, 178501), Christensen, Danon, and Scanlon note that they were unaware that publication of papers titled “Unified Scaling Law for Earthquakes” as an Arthur M. Sackler Colloquium paper in PNAS and as a letter in *Physical Review Letters* violated copyright transfer and double publication policies of the journals. These authors acknowledge significant overlap in data and figures between the two papers and apologize for their oversight.

www.pnas.org/cgi/doi/10.1073/pnas.0630527100

Development of ^{17}O NMR approach for fast imaging of cerebral metabolic rate of oxygen in rat brain at high field

Xiao-Hong Zhu, Yi Zhang, Run-Xia Tian, Hao Lei, Nanyin Zhang, Xiaoliang Zhang, Hellmut Merkle, Kamil Ugurbil, and Wei Chen[†]

Center for Magnetic Resonance Research, Department of Radiology, University of Minnesota Medical School, 2021 6th Street SE, Minneapolis, MN 55455

Communicated by Robert G. Shulman, Yale University, New Haven, CT, August 6, 2002 (received for review June 11, 2002)

A comprehensive technique was developed for using three-dimensional ^{17}O magnetic resonance spectroscopic imaging at 9.4T for rapidly imaging the cerebral metabolic rate of oxygen consumption (CMRO₂) in the rat brain during a two-min inhalation of $^{17}\text{O}_2$. The CMRO₂ value ($2.19 \pm 0.14 \mu\text{mol/g/min}$, $n = 7$) was determined in the rat anesthetized with α -chloralose by independent and concurrent ^{17}O NMR measurements of cerebral H_2^{17}O content, arterial input function, and cerebral perfusion. CMRO₂ values obtained were consistent with the literature results for similar conditions. Our results reveal that, because of its superior sensitivity at ultra-high fields, the ^{17}O magnetic resonance spectroscopic imaging approach is capable of detecting small dynamic changes of metabolic H_2^{17}O during a short inhalation of $^{17}\text{O}_2$ gas, and ultimately, for imaging CMRO₂ in the small rat brain. This study provides a crucial step toward the goal of developing a robust and noninvasive ^{17}O NMR approach for imaging CMRO₂ in animal and human brains that can be used for studying the central role of oxidative metabolism in brain function under normal and diseased conditions, as well as for understanding the mechanisms underlying functional MRI.

In the brain, the majority of energy consumption occurs by neuronal activity (1). This energy need is met predominantly through oxygen consumption mediated by the mitochondrial respiratory chain, coupled to oxidation of glucose as the main carbon source (2). The oxidative energy need of the human brain to sustain neuronal activity constitutes a large fraction of the energy requirements ($\approx 20\%$) in the entire body. The central role played by oxygen consumption is also evident in pathologies associated with the brain; perturbations in brain oxidative metabolism have been closely linked to many brain diseases such as schizophrenia, Alzheimer's disease, Huntington's disease, Parkinson's disease, and mitochondrial dysfunction, as well as aging problems (3–7). One line of evidence linking these diseases and cerebral oxidative metabolism is the histopathological finding that the activity of cytochrome oxidase, the key mitochondrial enzyme that catalyzes the reduction of oxygen to form water, is impaired in patients with schizophrenia (3) and Alzheimer's disease (4, 5).

Basal cerebral oxygen consumption is not uniform across different regions in the brain. It is recognized that capillary density in the brain is inhomogeneous (ref. 8 and refs. therein), suggesting that mitochondrial density, and hence, oxygen consumption are also likely to be inhomogeneous because a good correlation exists between capillarity and mitochondrial density in tissues (9). Alterations in neuronal activity due to stimulation or performance of a task increases this spatial nonuniformity by inducing regional changes in oxygen utilization as well as in blood flow and glucose consumption (10–12). In addition, the impairment in cytochrome oxidase content in the diseased brain was also found to affect different regions in the brain selectively (3–5). These considerations imply that the ability to *image* the cerebral metabolic rate of oxygen consumption (CMRO₂) *in vivo*

is essential for efforts aimed at investigating cerebral oxidative metabolism under normal and pathological conditions.

The earliest approach of CMRO₂ measurement is based on the Kety-Schmidt method for measuring cerebral blood flow (CBF) together with arteriovenous differences of oxygen content (13). This method, thought to be the most accurate one in the literature, provides only global CMRO₂ information without spatial differentiation within the brain. Positron emission tomography (PET) has been widely used for imaging CMRO₂ in humans (14–16). By introducing oxygen gas enriched with the isotope ^{15}O into the human body and monitoring the spatial distribution and accumulation rate of metabolic water (H_2^{15}O), PET can determine regional CMRO₂ and provide a CMRO₂ image. However, the ^{15}O -PET is unable to distinguish the radioactive signals between the ^{15}O molecule bound to hemoglobin and the ^{15}O atom incorporated into H_2^{15}O . To overcome this drawback, a measurement of cerebral blood volume using inhalation of C^{15}O has to be performed in addition to the CBF measurement based on *i.v.* injection of H_2^{15}O . These PET requirements make CMRO₂ measurements difficult to execute experimentally and complicate the calculation of CMRO₂ values.

The ^{13}C NMR methods based on monitoring the cerebral metabolism of intravenously infused [$1\text{-}^{13}\text{C}$] glucose (e.g., (10, 11, 17, 18)) provide an alternative approach for CMRO₂ measurements. The labeling kinetics for several intracellular metabolites, most importantly glutamate, can be unequivocally measured by these methods; extraction of CMRO₂ from experimental data relies on extensive modeling (10, 11, 18, 19). In addition, the ^{13}C NMR methods require a long measurement time (60–120 min) because of relatively slow turnover rates of cerebral metabolites, and it is difficult, although not impossible, to achieve three-dimensional (3D) CMRO₂ imaging because of a relatively long repetition time required for signal acquisitions.

The possibility of using the ^{17}O NMR spectroscopy/imaging techniques for monitoring labeled H_2^{17}O as a tracer of oxygen utilization or tissue perfusion have been introduced a decade ago (20–30). These early studies can be divided into two distinct groups. The first group involved the simple ^{17}O NMR approach for detecting H_2^{17}O directly (20, 21, 24–27). Nonlocalized ^{17}O NMR was used for most studies to estimate CMRO₂ in the whole brain of experimental animals as well as in the human occipital lobe (31) after inhalation of oxygen gas enriched with the ^{17}O isotope ($^{17}\text{O}_2$). Few studies attempted to obtain a coarse CMRO₂ image ($\geq 800 \mu\text{l}$ voxel size) in the cat brain with a long measurement time (25, 27). These previous efforts, all of which were conducted at relatively low fields compared with what is available currently, demonstrated the dramatic limitations imposed by the low inherent sensitivity of ^{17}O NMR due to its low

Abbreviations: CMRO₂, cerebral metabolic rate of oxygen; CBF, cerebral blood flow; PET, positron emission tomography; 3D, three-dimensional; MRS, magnetic resonance spectroscopic; SNR, signal-to-noise ratio.

[†]To whom reprint requests should be addressed. E-mail: wei@cmrr.umn.edu.

gyromagnetic ratio. These sensitivity limitations have hindered further developments of the ^{17}O NMR approach and lead to the exploration of a second group of methods that attempt to circumvent the sensitivity limitations of ^{17}O NMR by using indirect detection through ^{17}O -coupled protons.

The indirect ^{17}O detection approach relies on the effect of ^1H - ^{17}O scalar coupling on the transverse relaxation time (T_2) of the water protons, which is considerably shortened by the presence of the ^{17}O nucleus in the same water molecule (22). It has also been shown that the water proton T_2 of H_2^{17}O can be restored to that of H_2^{16}O when ^{17}O decoupling is applied; in this case, the difference between proton signals obtained with and without ^{17}O decoupling is related to the ^{17}O content of the water sample (28–30). However, the indirect ^{17}O measurements present difficulties for quantitatively correlating the proton signal changes to the concentrations of H_2^{17}O because the water T_2 is sensitive to many physiologic parameters such as pH and temperature. In addition, the fractional change in ^1H signal induced by variations in metabolic H_2^{17}O concentration is small at basal conditions. These indirect ^{17}O detection approaches have so far not been successful in imaging CMRO_2 quantitatively.

Recently, we have investigated the longitudinal and transverse relaxation times [T_1 , T_2 , and apparent T_2 (T_2^*)] as well as the signal-to-noise ratio (SNR) of ^{17}O spins in water by using the ^{17}O magnetic resonance spectroscopic (MRS) imaging method at 4.7T and 9.4T field strengths (32). Our results showed that the relaxation times of ^{17}O water are field-independent, and the ^{17}O NMR sensitivity increased approximately fourfold at 9.4T compared with a field strength of 4.7T. With this sensitivity gain, we were able to obtain two-dimensional ^{17}O MRS images of natural abundance H_2^{17}O in the rat brain at 9.4T with a temporal resolution of 12 s (32). These results demonstrated the potential of ^{17}O MRS imaging at ultra-high field for mapping the spatial distribution of metabolic H_2^{17}O dynamically in the rat brain.

In this study, we investigated the feasibility for developing the ^{17}O NMR approach for imaging CMRO_2 in a small animal model during a brief inhalation of $^{17}\text{O}_2$ gas. We have successfully applied the 3D ^{17}O MRS imaging method to determine CBF after a bolus injection of H_2^{17}O through an internal carotid artery and the accumulation rate of H_2^{17}O generated by oxidative metabolism in the rat brain during a two-min $^{17}\text{O}_2$ inhalation with superior spatial (27 μl) and temporal (11 s per 3D image) resolution. Furthermore, we performed experiments where such images were obtained together with continuous experimental monitoring of the arterial input function related to recirculated H_2^{17}O via an implanted carotid artery MR coil. These measurements were used to calculate CMRO_2 values rigorously in image voxels by using a complete modeling that accounts for all contributions to the cerebral H_2^{17}O content accumulated during an inhalation of $^{17}\text{O}_2$ and demonstrate the feasibility for imaging CMRO_2 . Based on these results, we present high-resolution 3D CMRO_2 images obtained with ^{17}O NMR under the basal condition in the rat brain anesthetized with α -chloralose.

Theory

The dynamic change of cerebral H_2^{17}O concentration accumulated during an inhalation of $^{17}\text{O}_2$ is determined by three processes: oxygen consumption generating metabolic H_2^{17}O in the brain, perfusion resulting in H_2^{17}O washout from the brain, and flow recirculation bringing extra H_2^{17}O into the brain. The mass balance equation of labeled H_2^{17}O concentrations during an inhalation of $^{17}\text{O}_2$ is given by

$$\frac{dC_b(t)}{dt} = 2\alpha f_1 \text{CMRO}_2 + \text{CBF}(f_2[C_a(t) - C_v(t)]), \quad [1]$$

where $C_a(t)$, $C_b(t)$, and $C_v(t)$ are the time-dependent H_2^{17}O concentrations expressed as $[\text{H}_2^{17}\text{O}]$ in excess of the natural

abundance $[\text{H}_2^{17}\text{O}]$ level in the arterial blood, brain tissue, and venous blood, respectively. The constant α is the enrichment fraction of ^{17}O -labeled O_2 gas. Proper use of Eq. 1 requires consistencies of units among all terms used in the equation. The determinations of C_b , C_a , and C_v are based on the ^{17}O NMR measurements and calibrated by using the natural abundance H_2^{17}O concentration (20.35 $\mu\text{mol}/(\text{g}$ of brain water) for brain tissue, and $\mu\text{mol}/(\text{g}$ of blood water) for blood, calculated from natural abundance H_2^{17}O enrichment of 0.037% and the molecular weight of $\text{H}_2^{17}\text{O} = 19.0$. Therefore, we prefer to use convenient units of $\mu\text{mol}/(\text{g}$ of brain water) for $C_b(t)$ and $\mu\text{mol}/(\text{g}$ of blood water) for $C_a(t)$ and $C_v(t)$. CMRO_2 is expressed in the conventional unit of $\mu\text{mol}/\text{min}/(\text{g}$ brain tissue) and is converted from the unit of $\mu\text{mol}/\text{min}/(\text{g}$ brain water) by using the conversion constant f_1 given by $f_1 = (\text{g}$ of brain tissue)/ $(\text{g}$ of brain water) = $1/\beta_{\text{brain}} = 1.266$, where β_{brain} is 0.79 (14, 27). The constant f_2 is also a unit conversion factor and is given by $f_2 = \rho_{\text{blood}}\beta_{\text{blood}}/\beta_{\text{brain}} = 1.05 \times 0.81/0.79 = 1.077$, where $\rho_{\text{blood}} = (\text{g}$ blood)/ $(\text{ml}$ blood) = 1.05 (33), and $\beta_{\text{blood}} = (\text{g}$ blood water)/ $(\text{g}$ blood) = 0.81 (14). If water in brain tissue is in equilibrium with water in venous blood (i.e., fast water exchange across capillaries), $f_2 C_v(t) = C_b(t)/\lambda$ where $\lambda = 0.90$ is the brain/blood partition coefficient with the unit of $(\text{ml}$ blood)/ $(\text{g}$ of brain tissue) (34). Substituting this relation and introducing two new correction parameters (n and m) into Eq. 1 leads to

$$\frac{dC_b(t)}{dt} = 2\alpha f_1 \text{CMRO}_2 + m \text{CBF} \left(f_2 C_a(t) - \frac{n C_b(t)}{\lambda} \right). \quad [2]$$

The solution of Eq. 2 is

$$C_b(t) = \frac{2\alpha\lambda f_1}{m n \text{CBF}} \text{CMRO}_2 \left[1 - e^{-\frac{m n \text{CBF}}{\lambda} t} \right] + f_2 m \text{CBF} \int_0^t C_a(t') e^{-\frac{m n \text{CBF}}{\lambda} (t-t')} dt', \quad [3]$$

where m is a correction factor accounting for the limited permeability of water because water is not freely diffusible across the brain-blood barrier; the value of m is 0.84 for the CBF range that we studied herein (35). The constant n is another correction factor that accounts for the additional restriction on the permeability of the H_2^{17}O generated through oxidative metabolism in the mitochondria (“metabolic” H_2^{17}O). This additional restriction is included in this modeling because we have observed that the washout rate of the metabolic H_2^{17}O after the cessation of $^{17}\text{O}_2$ inhalation was significantly slower than the washout rate of the H_2^{17}O that permeates brain tissue subsequent to a bolus injection of H_2^{17}O through the internal carotid artery in the rat.[‡] The cause of this difference could be permeability restrictions imposed by the inner and outer mitochondrial membranes that must be traversed by all water molecules generated by oxygen consumption. The ratio of the washout rate of the metabolic H_2^{17}O after the cessation of $^{17}\text{O}_2$ inhalation vs. the cerebral H_2^{17}O after a bolus injection of H_2^{17}O through the internal carotid artery gives the value of n . Limited permeability for the metabolic water has been reported in the human brain (36).

The CMRO_2 value can be precisely calculated by using Eq. 3 if all parameters of $C_b(t)$, CBF, and $C_a(t)$ can be experimentally measured for the same animal brain. The $C_b(t)$ and CBF values can be determined by using ^{17}O NMR approaches. To measure

[‡]Zhu, X. H., Lei, H., Zhang, Y., Zhang, X. L., Zhang, N. Y., Ugurbil, K. & Chen, W. (2002) *Proc. Int. Soc. Mag. Res. Med.* 10, 1094 (abstr.).

$C_a(t)$, we designed an implanted ^{17}O rf coil that permits the continuous measurement of $C_a(t)$ in a rat carotid artery. This measurement can be simultaneously performed with $C_b(t)$ measurement during an inhalation of $^{17}\text{O}_2$ by using separate rf channels on the MR spectrometer equipped with multiple receivers. In principle, the $C_a(t)$ function is determined by the metabolic H_2^{17}O generated in the entire animal body and the equilibration of this H_2^{17}O with the blood compartment. Considering that the oxygen consumption rate is constant (i.e., time independent) in all tissues during the short inhalation time, one can approximate $C_a(t)$ as a linear function of time [i.e., $C_a(t) = At$, where A is a constant]. This approximation was supported by our experimental results (see Fig. 5 presented later) and the literature. Then, the solution of Eq. 3 for CMRO_2 is

$$\text{CMRO}_2 = \frac{C_b(t) - \frac{Af_2\lambda^2}{mn^2\text{CBF}} \left(\frac{mn\text{CBF}}{\lambda} te^{-\frac{mn\text{CBF}}{\lambda}t} + e^{-\frac{mn\text{CBF}}{\lambda}t} - 1 \right)}{1 - e^{-\frac{mn\text{CBF}}{\lambda}t}} - \frac{Af_2\lambda t}{n} \cdot \frac{2\alpha\lambda f_1}{mn\text{CBF}} \quad [4]$$

Therefore, according to Eq. 4, the CMRO_2 value can be calculated by experimental data on CBF, A , n , $C_b(t)$, and other known constants (f_1 , f_2 , m , α , and λ) for each data point measured at different inhalation times for each voxel. All CMRO_2 values reported (except for those in Fig. 5) are averages of the values calculated as a function of time, excluding the first two time points because of their relatively large measurement errors and the fact that they may represent transient values during the approach to a steady-state rate of H_2^{17}O production by oxidative phosphorylation. Such transient values are expected during the build-up of $^{17}\text{O}_2$ in the brain at values that exceed the K_m of cytochrome oxidase for oxygen. Ability to obtain measurements as a function of time and the use of only the time independent values avoids this complication.

CBF values can be determined from the “washout” rate of the tracer H_2^{17}O in the brain tissue following a rapid bolus injection of H_2^{17}O through one carotid artery (32) according to Eq. 5:

$$C_b(t) = C_b(0)\exp[-t(m\text{CBF}/\lambda)], \quad [5]$$

where $C_b(0)$ is the cerebral H_2^{17}O concentration after the arrival of all labeled water after the bolus injection. Fitting the exponential decay of the H_2^{17}O washout curve according to Eq. 5 gives the CBF value.

Materials and Methods

NMR Methods. All NMR experiments were performed on a 9.4T/31-cm bore magnet (MagneX Scientific, Abingdon, U.K.) interfaced to a Unity INOVA console (Varian). A multinuclear head surface-coil probe consisting of a four-turn oval-shaped ^{17}O coil ($\approx 1 \text{ cm} \times 2 \text{ cm}$; 54.25 MHz) and a large butterfly-shaped ^1H coil (400 MHz) was used.

A TURBOFLASH (fast low-angle shot) image sequence was used to acquire scout images [TR/TE = 8 ms/4 ms, field of view (FOV) = 3 cm \times 3 cm, and image matrix size = 128 \times 128]. The spatial localization of ^{17}O MRS was achieved by using the 3D Fourier Series Window MRS imaging technique (32, 37). In this method, the k-space sampling is weighted according to the Fourier coefficients of a predetermined voxel shape to achieve an optimal filter applied at the acquisition stage. A cylindrical voxel shape (circular shape on the coronal orientation) was used in this study (37). Short T_1 value (4.5 ms) of cerebral H_2^{17}O in

the rat allows rapid signal acquisition, and ultimately, more signal averages within the same sampling time (32). Therefore, a short TR of 12 ms ($\approx 3T_1$) was used for gaining SNR. The acquisition time for each 3D ^{17}O -MRS image was 11 s (total scan number = 948; rf pulse width = 50 μs , spectral width = 30 kHz; FOV = 18 \times 18 \times 15 mm³, 9 \times 9 \times 5 phase encodes). Phase-encoding gradient was 0.35 ms long and had a half-sine waveform, which allowed for a short gradient echo time (TE = 0.4 ms). This short TE is critical for minimizing signal loss because of the relatively fast transverse relaxation of the ^{17}O magnetization ($T_2 = 3.0 \text{ ms}$ at 9.4T; ref. 32). The peak strength of the phase-encoding gradient increment was 0.09–0.11 G/cm. The image voxel size was 27 μl . A 17 \times 17 \times 9 matrix of free induction decay (FIDs) were generated from the original 9 \times 9 \times 5 phase encode data for each 3D ^{17}O image. The FIDs were zero-filled, and a 100-Hz line broadening (LB) was used before fast Fourier transformation for SNR enhancement. The ^{17}O NMR signals from each voxel were quantified by measuring the H_2^{17}O resonance peak intensities.

General Animal Preparation. Male Sprague–Dawley rats (250–300 g body weight) were anesthetized with $\approx 2\%$ (vol/vol) isoflurane in a mixture of O_2 and N_2O gases (2:3) during surgery. After oral intubations, femoral artery and vein were catheterized for physiological monitoring, blood sampling, and chemical administration. After surgery, anesthesia was switched to α -chloralose by using continuous infusion of 0.4 ml/hr of 15 mg/ml α -chloralose solution. Blood gases were sampled for monitoring physiological conditions [pH = 7.35 \pm 0.03, $\text{pCO}_2 = 42.1 \pm 3.0$ mmHg, $\text{pO}_2 = 124 \pm 16$ mmHg (1 mmHg = 133 Pa)]. The arterial blood pressure (80–110 mmHg) and EtCO_2 level ($\approx 3\%$) were monitored throughout the experiment. The rectal temperature of the rats was maintained at 37 \pm 1°C by using a heated water blanket. All animal surgical procedures and experimental protocols were conducted under the guidelines of the National Institutes of Health and the Institutional Animal Care and Use Committee of the University of Minnesota.

CBF Measurements. For CBF measurements, one external carotid artery was catheterized with a PE-50 tubing for gaining access to the internal carotid artery without interrupting blood circulation into the brain (32). A 0.05–0.1 ml 50%-enriched H_2^{17}O was rapidly injected into the brain through the internal carotid artery for CBF measurements using ^{17}O MRS imaging (32).

$C_a(t)$ Measurements. An implanted vascular rf coil was designed and constructed for continuously detecting the ^{17}O NMR signal changes of H_2^{17}O in the rat carotid artery at 9.4T. This coil was based on a modified solenoid coil design combined with an rf shielding.⁸ The rf shielding ensured that the NMR signal detected by the implanted coil was only attributed by the artery blood ($\approx 7 \mu\text{l}$) without contaminations from surrounding tissues. Therefore, additional spatial localization was not necessary for determining $C_a(t)$. In addition, the rf shielding minimized the electromagnetic coupling between the implanted ^{17}O coil and the head ^{17}O surface coil tuned at the same operating frequency (two-coil arrangement), which allowed simultaneous measurements of both $C_a(t)$ and $C_b(t)$ by using two receiver channels with the same temporal resolution (11 s).

$^{17}\text{O}_2$ Inhalation Experiments. For $^{17}\text{O}_2$ inhalation studies, the ^{17}O -labeled O_2 gas with 58.2–72.1% enrichment (Isotec) was mixed with N_2O gas ($\approx 2:3$) and then stored in a cylindrical gas reservoir. The 3D ^{17}O MRS imaging acquisitions were started

⁸Zhang, X. L., Tian, R. X., Zhu, X. H., Zhang, Y., Merkle, H. & Chen, W. (2002) *Proc. Int. Soc. Mag. Res. Med.* 10, 889 (abstr.).

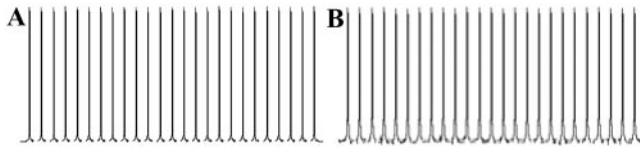


Fig. 1. (A) Stacked plot of 25 ^1H NMR spectra of natural abundance water in the rat brain acquired and processed with the following parameters: NT = 1, TR = 6.2s, LB = 25Hz (\approx half linewidth). The SD of the ^1H water peak height in these spectra is 0.20%. (B) Stacked plot of 25 ^{17}O NMR spectra of natural abundance water in the rat brain acquired and processed with the following parameters: NT = 512, TR = 12ms for each scan, LB = 100Hz (\approx half linewidth); the SD of the ^{17}O water peak height in these spectra is 0.35%. The total acquisition times for each ^1H and ^{17}O spectra were the same (6.2 s).

with the normal gas mixture first for 2 min; these natural abundance 3D ^{17}O MRS images were used as references for quantifications of metabolic H_2^{17}O concentrations in the rat brain during and after the $^{17}\text{O}_2$ inhalation. Subsequently, the respiration gas was quickly switched to the $^{17}\text{O}_2$ -labeled gas mixture. After 2 min of $^{17}\text{O}_2$ inhalation, the gas line was switched back to the normal gas mixture, and the 3D ^{17}O MRS imaging acquisitions were continued throughout the procedure; a total of 100 images were collected in about 19 min.

Determination of Constant n . The ratio between the washout rate of the metabolic H_2^{17}O after the cessation of $^{17}\text{O}_2$ inhalation and the washout rate of the H_2^{17}O trace from the H_2^{17}O bolus injected through the rat internal carotid artery gave the value of constant n for each voxel.

All results are presented as mean \pm SD.

Results

The multinuclear surface-coil probe was used to collect a series of global ^{17}O and ^1H spectra from the natural abundance water in the rat brain to estimate the relative signal fluctuations between ^{17}O and ^1H NMR. Two stacked plots of 25 ^{17}O and ^1H spectra acquired consecutively by using the ^{17}O coil and the much larger ^1H coil, respectively, are shown in Fig. 1. Although the number of acquisitions (NT) for each spectrum was different for the ^{17}O and ^1H nuclei, the repetition time (TR) was $\approx 3T_1$ in both cases; the total acquisition time was 6.2 s for all spectra. Under this condition, we found that the signal fluctuations in the consecutively acquired spectra for the two nuclei were comparable (SD = 0.20% for ^1H spectra; SD = 0.35% for ^{17}O spectra). This result demonstrates that with respect to the capability for detecting fractional changes in NMR signal intensity, the ^{17}O method is comparable to the ^1H method.

The 3D ^{17}O MRS imaging technique was applied to measure the natural abundance H_2^{17}O distribution in the rat brain with high temporal resolution of 11 s and spatial resolution ($27 \mu\text{l}$ voxel size). Fig. 2A shows representative data obtained from three adjacent coronal images in a rat brain showing anatomical images acquired by the ^1H coil and the ^{17}O MRS images of natural abundance H_2^{17}O acquired by the ^{17}O coil. Fig. 2B displays one ^{17}O chemical shift image from the middle image slice as shown in Fig. 2A. The spatial distributions of ^{17}O NMR signal intensity are not uniform because of the inhomogeneous B_1 of the ^{17}O surface coil. Nevertheless, excellent SNR was achieved with a relatively short acquisition time at 9.4T, especially for the central voxels where SNR was optimized by the B_1 profile of the ^{17}O coil (SNR $\approx 40:1$).

The large sensitivity gained at ultra-high field revealed the potential of ^{17}O MRS imaging for detecting small dynamic changes of cerebral H_2^{17}O in small animal brains during a short inhalation of $^{17}\text{O}_2$. Fig. 3 demonstrates stacked plots of ^{17}O spectra of cerebral H_2^{17}O from one representative voxel before (natural abundance),

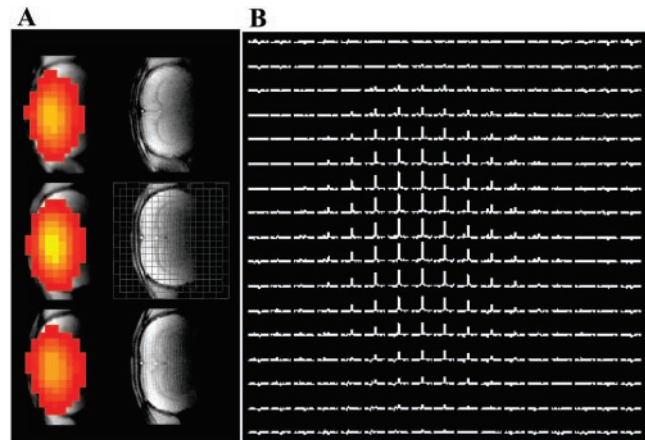


Fig. 2. (A) 3D ^{17}O brain images of natural abundance H_2^{17}O from three adjacent slices (Left, color images) and corresponding anatomical images (Right, gray images) in the coronal orientation from a representative rat. (B) Chemical shift image of natural abundance H_2^{17}O from Middle as shown in A.

during, and after a 2-min inhalation of $^{17}\text{O}_2$ (72.1% ^{17}O enrichment). It is clearly evident that the ^{17}O signal intensity of cerebral H_2^{17}O in the entire measurement is characterized by three distinct phases: (i) constant before the $^{17}\text{O}_2$ inhalation; (ii) approximately linearly increasing during the $^{17}\text{O}_2$ inhalation; and (iii) decreasing after the cessation of $^{17}\text{O}_2$ inhalation, approximately exponentially, and reaching a new steady state within a short time (<10 min).

When the cerebral H_2^{17}O concentrations reached a new steady state after the $^{17}\text{O}_2$ inhalation experiment, the CBF measurement was performed by a rapid bolus injection of H_2^{17}O into one internal carotid artery. The dynamic distribution of cerebral H_2^{17}O signal during the washout period was monitored by using 3D ^{17}O MRS imaging. The washout curves excluding the first data point were fitted to an exponential decay function according to Eq. 5, and these fits yielded CBF values. Fig. 4 demonstrates one example of CBF measurement obtained from the same rat and image voxel used in Fig. 3 showing the stacked plot of ^{17}O spectra and the exponential fit. Because the H_2^{17}O bolus was injected into one of the internal carotid arteries, and the H_2^{17}O tracer was mainly distributed into the ipsilateral hemisphere, CBF and, subsequently, CMRO_2 quantifications were performed only for the ^{17}O image voxels in the ipsilateral hemisphere of the rat brain.

Fig. 5A illustrates the natural abundance H_2^{17}O spectrum from the blood in the rat carotid artery. Fig. 5B plots the results of simultaneous measurements of $C_a(t)$ change in one carotid artery and $C_b(t)$ change in a voxel in the ipsilateral hemisphere

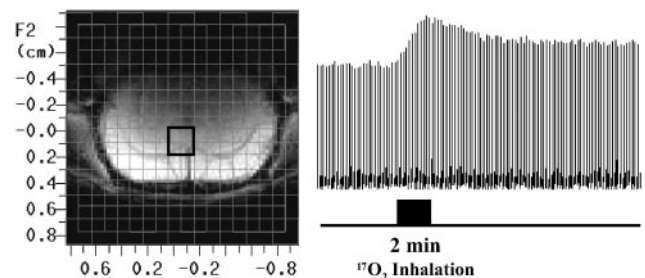


Fig. 3. Stacked plots of the cerebral H_2^{17}O spectra from one representative voxel ($27 \mu\text{l}$ voxel size) as indicated in the anatomical image (Left Inset) acquired before (natural abundance), during (as indicated by the dark bar under the stacked plots) and after a 2-min $^{17}\text{O}_2$ inhalation.

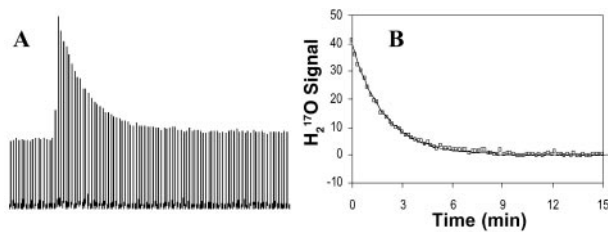


Fig. 4. (A) Stacked plots of the cerebral H_2^{17}O spectra from one voxel (used in Fig. 3) after a fast bolus injection of H_2^{17}O into the rat brain through an internal carotid artery. (B) Exponential decay fitting of the H_2^{17}O washout curve for calculating CBF (0.56 ml/g/min for this voxel).

brain during an inhalation of $^{17}\text{O}_2$. The $C_a(t)$ data were fitted by a linear function for calculating the value of constant A. Finally, the values of $C_b(t)$, CBF, and n from each voxel and the value of A measured from each ^{17}O inhalation measurement were used to calculate CMRO_2 according to Eq. 4. Fig. 5C demonstrates one example of CMRO_2 calculations as a function of time from a single voxel. It is evident in Fig. 5C that the CMRO_2 value is independent of the inhalation time if the initial two points are excluded. The averaged CMRO_2 values (excluding two initial points) and CBF values from seven measurements are $2.19 \pm 0.14 \mu\text{mol/g/min}$ and $0.53 \pm 0.07 \text{ ml/g/min}$, respectively, in the rat brains anesthetized with α -chloralose.

The mean CBF and n values obtained from the entire hemisphere ipsilateral to the internal carotid artery where a H_2^{17}O bolus was injected were subsequently used to calculate CMRO_2 values for both ipsilateral and contralateral hemispheres approximately and to obtain 3D CMRO_2 images. This approximation was made based on the fact that the CBF distribution in the hemisphere where it was measured was relatively uniform and that two hemispheres should be equivalent with respect to CBF. Fig. 6 illustrates three adjacent CMRO_2 images in the coronal orientation from a representative rat brain. The inhomogeneous signal intensity caused by the surface coil sensitivity profile (Fig. 2) is not reflected in the CMRO_2 maps, as expected.

Discussion

The ^{17}O T_1 value in H_2^{17}O is less than 5 ms in the rat brain at 9.4T (32). This short T_1 permits much faster data acquisitions, more signal averages, and, consequently, a high SNR per unit of time. This advantage is critical for the success of CMRO_2 measurement using direct ^{17}O detection. The comparable fractional signal fluctuations between consecutively acquired ^1H and ^{17}O NMR spectra (Fig. 1) indicated that direct ^{17}O detection of changes in metabolic H_2^{17}O signal is likely to be more sensitive than the indirect ^{17}O detection through ^1H NMR. This notion is based on the fact that the fractional change of water proton signal caused by a 2-min $^{17}\text{O}_2$ inhalation at basal condition is

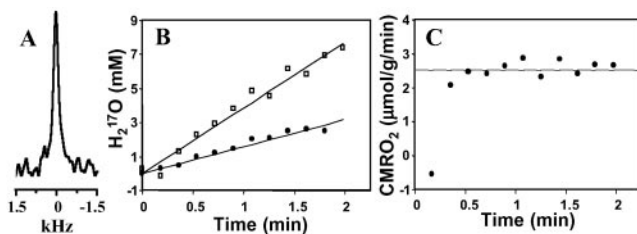


Fig. 5. (A) Natural abundance ^{17}O spectrum of H_2^{17}O in the rat carotid artery blood ($7 \mu\text{l}$) obtained before inhalation of $^{17}\text{O}_2$. (B) Time course of ^{17}O MR signals of $C_a(t)$ in one carotid artery (\bullet) and $C_b(t)$ from a representative voxel in the rat brain (\square) during inhalation of $^{17}\text{O}_2$. (C) Plot of the calculated CMRO_2 values using the complete modeling as described by Eq. 4 as a function of time.



Fig. 6. 3D coronal CMRO_2 images of rat brain measured during a 2-min $^{17}\text{O}_2$ inhalation.

estimated to be 0.15–0.30% (29), which is difficult to detect reliably because this change is comparable to the signal fluctuations in consecutively acquired ^1H spectra or images. These signal fluctuations are not dominated by the inherent SNR of a single spectrum or image but are mainly determined by the physiological processes of breathing, heart pulsation, and vasomotion, as well as NMR scanner instability. In contrast, ^{17}O NMR has a much larger dynamic range for detecting the changes of metabolic H_2^{17}O (20–40%) during the same $^{17}\text{O}_2$ inhalation. This difference is the major merit that makes ^{17}O NMR more suitable for CMRO_2 imaging.

The ^{17}O approach has several major advantages for CMRO_2 imaging in comparison with other existing methods. First, ^{17}O NMR can specifically detect metabolic H_2^{17}O without confounding signals from the $^{17}\text{O}_2$ bound to hemoglobin or $^{17}\text{O}_2$ dissolved in tissue space. When bound to hemoglobin, the $^{17}\text{O}_2$ resonance is broadened beyond detection because of the slow rotational motion for the large molecular weight oxyhemoglobin complex. $^{17}\text{O}_2$ as an unbound molecule in gas phase or dissolved in water is strongly paramagnetic because of its unpaired electrons and, hence, undetectable because of the dipolar coupling between the electrons and the nucleus. As a result, ^{17}O NMR avoids the complication in the calculation of CMRO_2 encountered in the PET methodology. In addition, unlike PET, the ^{17}O isotope is stable and nonradioactive, and the experimental procedure of $^{17}\text{O}_2$ inhalation does not introduce any physiological perturbation and complexities in the animal. These merits can significantly simplify the modeling of CMRO_2 calculation as well as provide an approach for imaging CMRO_2 in living organs with minimal biological risk. Second, the natural abundance signal of H_2^{17}O , which can be accurately imaged, provides an internal reference for rigorously calibrating and calculating the absolute H_2^{17}O concentration changes for both $C_b(t)$ and $C_a(t)$ during $^{17}\text{O}_2$ inhalation; such a quantification is crucial for determining absolute CMRO_2 values and is independent of the inhomogeneities of ^{17}O coil sensitivity. Third, there is only a single and well defined ^{17}O resonance peak of H_2^{17}O , thus making spectral analysis simple. Fourth, the ^{17}O resonance peak is relatively broad and has a low resonance frequency (only 14% of the ^1H resonance frequency); hence, it is significantly less sensitive to static magnetic field inhomogeneities. Fifth, after the cessation of $^{17}\text{O}_2$ inhalation, the cerebral H_2^{17}O concentration reaches a new steady state within a short time (6–10 min); this fast recovery should allow repeated CMRO_2 measurements in the same subject and same experimental session. This capability is essential for studying the oxidative metabolism changes related to perturbations in physiology and function, where at least two measurements are required under control and perturbation conditions. Finally, at ultra-high fields the ^{17}O NMR sensitivity is adequate to obtain relatively high-resolution images, even relative to the small size of the rat brain, with an 11-s acquisition time; this sensitivity makes the ^{17}O approach possible for imaging CMRO_2 within a short measurement duration (2 min).

Because of the technical challenges faced for most existing CMRO_2 imaging methods, there is virtually no literature reporting direct measurements of CMRO_2 in the rat brain. For instance, the image voxel size of most conventional PET scanners is on the order of several milliliters (e.g., ref. 38); this size is already larger than the size of the entire rat brain. Nevertheless, we compared our result of CMRO_2 measurement by using

the ^{17}O NMR approach with the literature results obtained by indirect methods under similar condition. Based on an autoradiographic approach (39), cerebral metabolic rate of glucose (CMR_{glc}) was recently determined to be $\approx 0.37 \mu\text{mol/g/min}$ in the somatosensory and motor cortices of rats anesthetized with α -chloralose. By using the $\text{CMRO}_2/\text{CMR}_{\text{glc}}$ ratio of 5.5 (2), a CMRO_2 value of $2.04 \mu\text{mol/g/min}$ is calculated from this CMR_{glc} measurement, which is in excellent agreement with our ^{17}O -based CMRO_2 result ($2.19 \pm 0.14 \mu\text{mol/g/min}$). The CBF value of $0.58\text{--}0.68 \text{ ml/g/min}$ reported in the same autoradiographic study (39) is also close to the mean CBF value of $0.53 \pm 0.07 \text{ ml/g/min}$ measured in our study. The heteronuclear editing MRS and ^1H MRI methods covering a large range of cortical activity at different anesthesia conditions had been used to measure CMRO_2 and CBF values in the sensory motor cortex of mature rats, and a linear correlation between CMRO_2 and CBF was observed ($\text{CMRO}_2 = 3.76 \cdot \text{CBF} + 0.18$, $R^2 = 0.99$; ref. 40). The estimated CMRO_2 from this relation is $2.16 \mu\text{mol/g/min}$ if the CBF value observed in our study (0.53 ml/g/min) is applied. This CMRO_2 value is again in excellent agreement with our result. These comparisons provide mutual support between our direct CMRO_2 measurements and other indirect measurements reported in the literature and support the validity of the 3D CMRO_2 imaging using ^{17}O NMR.

The CMRO_2 measurements presented in this paper involved two invasive procedures: one for determining $\text{C}_a(t)$ by means of the implanted ^{17}O rf coil, and the second for measuring CBF by an intra-arterial catheter and bolus injection of H_2^{17}O . The CBF measurement can be performed noninvasively by using the arterial spin tagging MR approaches (41). The implanted rf coil, on the other hand, is not practical for routine measurements of CMRO_2 by using small experimental animal models (e.g., rat or mouse), nor is it suitable for human applications. Therefore, it would be important to explore further the feasibility of the ^{17}O NMR

approach for reliably imaging CMRO_2 without resorting to invasive $\text{C}_a(t)$ measurements. A successful outcome from such a study will establish a completely noninvasive ^{17}O approach for CMRO_2 imaging.

In comparison with most existing approaches, the high-field ^{17}O NMR method requires a significantly short measurement time for imaging CMRO_2 and can be performed within a 2-min $^{17}\text{O}_2$ inhalation period. However, this method assumes that CMRO_2 is constant during the measurement. SNR considerations suggest that the CMRO_2 measurement time can further shorten at 9.4T or higher magnetic fields. Although rapid dynamic changes of CMRO_2 that occur faster than this time-scale will be beyond the reach of this method, this time-scale is faster than any other technique currently available for assessing CMRO_2 , especially at the spatial resolution available from the ^{17}O NMR approach.

Conclusion

We have successfully developed a comprehensive technique by using ^{17}O MRS imaging at ultra-high field for fast imaging of CMRO_2 in the rat brain and validated it with complementary measurements. The overall results from our study provide an essential step toward the goal for developing a robust, fast, reliable, and noninvasive ^{17}O NMR approach for imaging the rate of oxidative metabolism for both animal and human brains and, potentially, for other living organs. Such an approach would be useful for studying the central role of oxidative metabolism in brain function under normal and diseased conditions, as well as for understanding the mechanisms underlying functional MRI (42).

We thank Dr. Jae-Hwan Kwag and John Strupp for their technical assistance and Dr. Haiying Liu for scientific discussions. This work was supported by National Institutes of Health Grants NS41262, NS38070, NS39043, and EB00329; National Research Resource Grant P41 RR08079 (from the National Institutes of Health); the MIND Institute; and the W. M. Keck Foundation.

- Atwell, D. & Laughlin, S. B. (2001) *J. Cereb. Blood Flow Metab.* **21**, 1133–1145.
- Siesjo, B. K. (1978) *Brain Energy Metabolism* (Wiley, New York).
- Maurer, I., Zierz, S. & Moller, H. (2001) *Schizophr. Res.* **48**, 125–136.
- Wong-Riley, M., Antuono, P., Ho, K. C., Egan, R., Hevner, R., Liebl, W., Huang, Z., Rachel, R. & Jones, J. (1997) *Vision Res.* **37**, 3593–3608.
- Maurer, I., Zierz, S. & Moller, H. J. (2000) *Neurobiol. Aging* **21**, 455–462.
- Frackowiak, R. S., Herold, S., Petty, R. K. & Morgan-Hughes, J. A. (1988) *Brain* **111**, 1009–1024.
- Beal, M. F. (1992) *Ann. Neurol.* **31**, 119–130.
- Harrison, R. V., Harel, N., Panesar, J. & Mount, R. J. (2002) *Cereb. Cortex* **12**, 225–233.
- Hoppeler, H. & Kayar, S. R. (1988) *News Physiol. Sci.* **3**, 113–116.
- Hyder, F., Chase, J. R., Behar, K. L., Mason, G. F., Siddeek, M., Rothman, D. L. & Shulman, R. G. (1996) *Proc. Natl. Acad. Sci. USA* **93**, 7612–7617.
- Chen, W., Zhu, X. H., Gruetter, R., Seaquist, E. R. & Ugurbil, K. (2001) *Magn. Reson. Med.* **45**, 349–355.
- Raichle, M. E. (1987) in *Handbook of Physiology—The Nervous System*, eds Mountcastle, V. B., Plum, F. & Geiger, S. R. (Am. Physiol. Soc., Washington, DC), pp. 643–674.
- Kety, S. S. & Schmidt, C. F. (1948) *J. Clin. Invest.* **27**, 476–483.
- Ter-Pogossian, M. M., Eichling, J. O., Davis, D. O. & Welch, M. J. (1970) *J. Clin. Invest.* **49**, 381–391.
- Mintun, M. A., Raichle, M. E., Martin, W. R. & Herscovitch, P. (1984) *J. Nucl. Med.* **25**, 177–187.
- Lenzi, G. L., Frackowiak, R. S., Jones, T., Heather, J. D., Lammertsma, A. A., Rhodes, C. G. & Pozzilli, C. (1981) *Eur. Neurol.* **20**, 285–290.
- Rothman, D. L., Novotny, E. J., Shulman, G. I., Howseman, A. M., Petroff, O. A., Mason, G., Nixon, T., Hanstock, C. C., Prichard, J. W. & Shulman, R. G. (1992) *Proc. Natl. Acad. Sci. USA* **89**, 9603–9606.
- Gruetter, R., Seaquist, E. R. & Ugurbil, K. (2001) *Am. J. Physiol.* **281**, E100–E112.
- Mason, G. F., Rothman, D. L., Behar, K. L. & Shulman, R. G. (1992) *J. Cereb. Blood Flow Metab.* **12**, 434–447.
- Mateescu, G. D., Yvars, G. M. & Dular, T. (1988) in *Water and Ions in Biological Systems*, eds Lauger, P., Packer, L. & Vasilescu, V. (Birkhauser, Basel), pp. 239–250.
- Mateescu, G. D., Yvars, G., Pazara, D. I., Alldridge, N. A., LaManna, J. C., Lust, D. W., Mattingly, M. & Kuhn, W. (1989) in *Synthesis and Application of Isotopically Labeled Compounds*, eds Baillie, T. A. & Jones, J. R. (Elsevier, Amsterdam), pp. 499–508.
- Hopkins, A. L. & Barr, R. G. (1987) *Magn. Reson. Med.* **4**, 399–403.
- Kwong, K. K., Hopkins, A. L., Belliveau, J. W., Chesler, D. A., Pong, K. K., McInstry, R. C., Finelli, D. A., Hunter, G. J., Moore, J. B., Barr, R. G. & Rosen, B. R. (1991) *Magn. Reson. Med.* **22**, 154–158.
- Arai, T., Nakao, S., Mori, K., Ishimori, K., Morishima, I., Miyazawa, T. & Fritz-Zieroth, B. (1990) *Biochem. Biophys. Res. Commun.* **169**, 153–158.
- Pekar, J., Ligeti, L., Ruttner, Z., Lyon, R. C., Sinnwell, T. M., van Gelderen, P., Fiat, D., Moonen, C. T. & McLaughlin, A. C. (1991) *Magn. Reson. Med.* **21**, 313–319.
- Fiat, D., Ligeti, L., Lyon, R. C., Ruttner, Z., Pekar, J., Moonen, C. T. & McLaughlin, A. C. (1992) *Magn. Reson. Med.* **24**, 370–374.
- Pekar, J., Sinnwell, T., Ligeti, L., Chesnick, A. S., Frank, J. A. & McLaughlin, A. C. (1995) *J. Cereb. Blood Flow Metab.* **15**, 312–320.
- Ronen, I. & Navon, G. (1994) *Magn. Reson. Med.* **32**, 789–793.
- Ronen, I., Merkle, H., Ugurbil, K. & Navon, G. (1998) *Proc. Natl. Acad. Sci. USA* **95**, 12934–12939.
- Reddy, R., Stolpen, A. H. & Leigh, J. S. (1995) *J. Magn. Reson.* **108**, 276–279.
- Fiat, D., Dolinsek, J., Hankiewicz, J., Dujovny, M. & Ausman, J. (1993) *Neurol. Res.* **15**, 237–248.
- Zhu, X. H., Merkle, H., Kwag, J. H., Ugurbil, K. & Chen, W. (2001) *Magn. Reson. Med.* **45**, 543–549.
- Altman, P. L. (1961) in *Biological Handbook Series* (Fed. Am. Soc. Exper. Biol., Washington, DC), p. 14.
- Herscovitch, A. & Raichle, M. E. (1985) *J. Cereb. Blood Flow Metab.* **5**, 65–69.
- Herscovitch, P., Raichle, M. E., Kilbourn, M. R. & Welch, M. J. (1987) *J. Cereb. Blood Flow Metab.* **7**, 527–542.
- Ohta, S., Meyer, E., Thompson, C. J. & Gjedde, A. (1992) *J. Cereb. Blood Flow Metab.* **12**, 179–192.
- Hendrich, K., Hu, X., Menon, R., Merkle, H., Camarata, P., Heros, R. & Ugurbil, K. (1994) *J. Magn. Reson.* **105**, 225–232.
- Fox, P. T., Raichle, M. E., Mintun, M. A. & Dence, C. (1988) *Science* **241**, 462–464.
- Nakao, Y., Itoh, Y., Kuang, T. Y., Cook, M., Jehle, J. & Sokoloff, L. (2001) *Proc. Natl. Acad. Sci. USA* **98**, 7593–7598.
- Hyder, F., Kennan, R. P., Kida, I., Mason, G. F., Behar, K. L. & Rothman, D. (2000) *J. Cereb. Blood Flow Metab.* **20**, 485–498.
- Detre, J. A., Zhang, W., Roberts, D. A., Silva, A. C., Williams, D. S., Grandis, D. J., Koretsky, A. P. & Leigh, J. S. (1994) *NMR Biomed.* **7**, 75–82.
- Barinaga, M. (1997) *Science* **276**, 196–198.